

1 **U-Pb dating of middle Eocene-Pliocene multiple tectonic pulses in the Alpine**  
2 **foreland**

3

4 **Luca Smeraglia<sup>1,2,3</sup>, Nathan Looser<sup>4\*</sup>, Olivier Fabbri<sup>2</sup>, Flavien Choulet<sup>2</sup>, Marcel Guillong<sup>4</sup>,**  
5 **Stefano M. Bernasconi<sup>4</sup>**

6

7 1. National Research Council, IGAG, Rome, Italy

8 2. Chrono-Environnement, UMR 6249, Université de Bourgogne-Franche Comté, 25000 Besançon, France

9 3. formerly at Dipartimento di Scienze della Terra, Sapienza Università di Roma, P.le Aldo Moro 5, 00185, Roma

10 4. Geological Institute, ETH Zürich, Sonneggstrasse 5, 8092 Zürich, Switzerland

11

12 \*Corresponding author e-mail address: [Nathan.looser@erdw.ethz.ch](mailto:Nathan.looser@erdw.ethz.ch)

13

14 **Abstract.** Foreland fold-and-thrust belts record long-lived tectono-sedimentary activity, from passive  
15 margin sedimentation, flexuring, and further involvement into wedge accretion ahead of an advancing  
16 orogen. Therefore, dating fault activity is fundamental for plate movement reconstruction, resource  
17 exploration or earthquake hazard assessment. Here, we report U-Pb ages of syntectonic calcite  
18 mineralizations from four thrusts and three tear faults sampled at the regional scale, across the Jura  
19 fold-and-thrust belt in the northwestern Alpine foreland (eastern France). Three regional tectonic  
20 phases are recognized in the middle Eocene-Pliocene interval: (1) pre-orogenic faulting at  $48.4 \pm 1.5$   
21 and  $44.7 \pm 2.6$  Ma associated to the far-field effect of the Alpine or Pyrenean compression, (2) syn-  
22 orogenic thrusting at  $11.4 \pm 1.1$ ,  $10.6 \pm 0.5$ ,  $9.7 \pm 1.4$ ,  $9.6 \pm 0.3$ , and  $7.5 \pm 1.1$  Ma associated to the  
23 formation of the Jura fold-and-thrust belt with possible in-sequence thrust propagation, and (3) syn-  
24 orogenic tear faulting at  $10.5 \pm 0.4$ ,  $9.1 \pm 6.5$ ,  $5.7 \pm 4.7$ , and at  $4.8 \pm 1.7$  Ma including the reactivation  
25 of a pre-orogenic fault at  $3.9 \pm 2.9$  Ma. Previously unknown faulting events at  $48.4 \pm 1.5$  and  $44.7 \pm$   
26  $2.6$  Ma predate by  $\sim 10$  Ma the reported late Eocene age for tectonic activity onset in the Alpine

27 foreland. In addition, we date the previously inferred re-activation of pre-orogenic strike-slip faults  
28 as tear faults during Jura imbrication. The U-Pb ages document a minimal time frame for the evolution  
29 of the Jura FTB wedge by possible in-sequence thrust imbrication above the low-friction basal  
30 décollement consisting of evaporites.

31

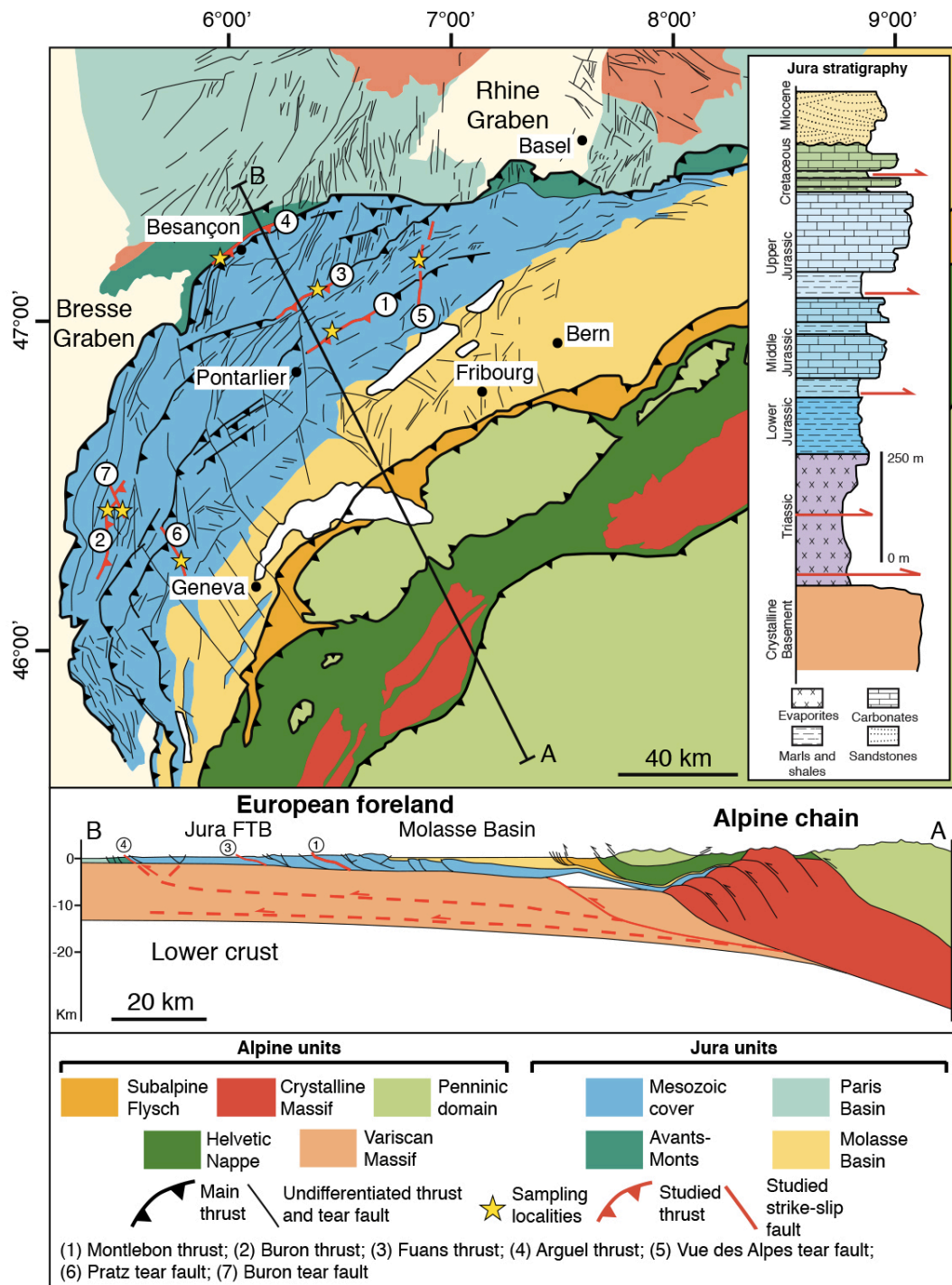
## 32 **1. Introduction**

33 Foreland fold-and-thrust belts develop at the external edges of orogens and are characterized  
34 by a multiphase tectono-sedimentary history including: pre-orogenic sedimentation, uplift at the  
35 peripheral bulge of the advancing orogen, progressively accelerating subsidence followed by syn-  
36 tectonic sedimentation, and accretion of the sedimentary cover into the foreland fold-and-thrust belt  
37 (Lacombe et al., 2007). Unraveling the timing of these tectonic events is fundamental for plate  
38 kinematic modelling, natural resource exploration, paleoseismicity, and topography evolution studies  
39 (Vergés et al., 1992; Craig and Warvakai, 2009). However, deciphering the different tectonic phases  
40 is complicated by the overprinting of inherited structures by progressively younger tectonic events.

41 This issue is addressed by dating syn-tectonic sediments and, more recently, better constrained  
42 through dating of fault activity with K-Ar,  $^{40}\text{Ar}/^{39}\text{Ar}$ , and U-Pb and U-Th methods (Van der Pluijm  
43 et al., 2009; Vrolijk et al., 2018). In particular, calcite U-Pb and U-Th geochronology (Roberts et al.,  
44 2020) is the unique method for dating syntectonic calcite mineralizations. This technique has been  
45 applied for dating single faults in extensional, strike-slip, and compressional settings (Goodfellow et  
46 al., 2017; Nuriel et al., 2017; Hansman et al., 2018; Smeraglia et al., 2019; Carminati et al., 2020).  
47 So far, the dating of multiple faults at the regional scale across a foreland fold-and-thrust belt remains  
48 rare (Beaudoin et al., 2018; Looser et al., 2021).

49 In this study, we dated syntectonic calcite mineralizations from four thrusts and three tear faults  
50 sampled across the Jura fold-and-thrust belt (Jura FTB, eastern France, Fig. 1) by laser ablation  
51 inductively coupled plasma mass spectrometry (LA-ICP-MS) U-Pb dating. We reconstructed three  
52 tectonic phases having occurred in the middle Eocene-Pliocene period, documenting a long-lived

53 polyphase tectonic history of the northwestern Alpine foreland system along the convergent boundary  
 54 between European and African plates.



55  
 56 **Figure 1.** Geological map of the northwestern Alpine foreland and surrounding areas and stratigraphic column of the  
 57 main lithological units of the Jura area. [Map m](#) modified from [Rime et al. \(2019\)](#), [cross-section modified from Von Hagke](#)  
 58 [et al., 2014](#).

59 **2. Tectonic setting**

60 Located in the Western Alps foreland, the Jura FTB formed by the ongoing continental collision  
61 of the Eurasian plate with the African plate (Sommaruga, 1997; Mosar, 1999; Lacombe and  
62 Mouthereau, 2002; Affolter and Gratier 2004; Bellahsen et al., 2014) (Fig. 1). Shortening affected the  
63 Triassic-late Miocene sedimentary succession deposited on the European passive margin above the  
64 Hercynian crystalline basement and caused brittle-ductile deformation at several levels (Fig. 1)  
65 (Philippe et al., 1996; Homberg et al., 2002; Ustaszewski and Schmid, 2006). The sedimentary  
66 succession starts with Triassic shales and evaporites overlain by Jurassic-Cretaceous shales, marls,  
67 and limestones (Fig. 1) (Sommaruga et al., 2017). Following a Late Cretaceous-Eocene regional  
68 unconformity, Oligocene-Miocene shallow marine to continental clastic deposits of the Molasse  
69 Basin were deposited above Cretaceous limestones (Fig. 1).

70 The post-Mesozoic tectonic history of the Jura area is assumed to have started in the middle  
71 Eocene with N-S shortening related to the far field effect of the "Pyrenean orogeny" generating strike-  
72 slip faults (Bergerat, 1987). However, no absolute ages of this tectonic phase are available. Based on  
73 structural analyses and calcite U-Pb ages, three phases of normal faulting during the Late Eocene,  
74 Oligocene, and Miocene in the distal parts of the Molasse Basin in northern Switzerland and in the  
75 Jura area have been documented (Lacombe et al., 1993; Homberg et al., 2002; Mazurek et al., 2018;  
76 Radaideh and Mosar, 2021). Normal faulting during the Late Eocene-Oligocene is associated to  
77 crustal extension due to the opening of the Rhine Graben (Lacombe et al., 1993; Homberg et al.,  
78 2002; Mazurek et al., 2018; Radaideh and Mosar, 2021) or to the coeval onset of Alpine collision  
79 (Merle and Michon, 2001), while normal faulting during the middle Miocene has been related to  
80 crustal tilting associated to uplift of the Black Forest Highlands and subsidence of the northern part  
81 of the Molasse Basin (Mazurek et al., 2018).

82 Biostratigraphic dating of syn-orogenic deposits, geomorphological observations,  
83 interpretation of seismic reflection profiles, and syntectonic calcite U-Pb ages of fault activity in the  
84 eastern tip of Jura FTB indicate that orogenic shortening started ~14.5 Ma ago (Langhian times) at  
85 the latest (Looser et al., 2021 and references therein) and is still active (Mosar, 1999; Becker, 2000;

86 [Lacombe and Mouthereau, 2002](#); [Madritsch et al., 2008](#)). Shortening was accommodated by N to NE-  
87 verging and NE-SW-striking thrusts and by NW-SE to N-S trending sinistral tear faults ([Sommaruga,](#)  
88 [1997](#)) ([Fig. 1](#)). The main décollement level of the thrust system developed along Triassic evaporites  
89 ([Jordan, 1992](#); [Pfiffner, 2014](#); [Gruber, 2017](#); [Sommaruga et al., 2017](#)). Therefore, there is a common  
90 agreement in considering the Jura FTB mainly as the product of thin-skinned tectonics ([Sommaruga,](#)  
91 [1997](#)). However, thick-skinned tectonics occurred in the late stage of deformation, mostly in the  
92 external part ([Lacombe and Mouthereau, 2002](#); [Ustaszewski and Schmid, 2006, 2007](#); [Madritsch et](#)  
93 [al., 2008](#); [Lacombe and Bellahsen, 2016](#)).

94 Field cross-cutting relationships and U-Pb ages of syntectonic calcite mineralizations show that  
95 tear faults were synchronously active with thrusting and folding ([Sommaruga, 1997](#); [Looser et al.,](#)  
96 [2021](#)) and their movement continued after thrusting. In fact, in some cases, tear faults are still  
97 seismogenic ([Thouvenot et al., 1998](#)). Several authors suggested that pre-orogenic strike-slip and  
98 normal faults were reactivated in early Pliocene, respectively as tear and transpressional faults  
99 ([Madritsch et al., 2008](#); [Hombert et al., 1997](#); [Ustaszewski and Schmid, 2006](#)). Overall, direct dating  
100 of this fault reactivation is so far not available.

101

### 102 **3. Methods**

103 The following methods were used: (1) field structural analyses and vein/slickenside sampling  
104 from four major thrusts (From SE to NW: Montlebon, Buron, Fuans, and Arguel thrusts) and three  
105 NNE-SSW tear faults (Vue des Alpes, Pratz, and Buron) moving from the internal (most deformed)  
106 to the external (less deformed) parts of the Jura FTB ([Fig. 1](#)). In particular, we measured the  
107 orientation of sampled veins and the rake of sampled slickensides in order to combine U-Pb ages  
108 from veins and slickensides with structural measurements; (2) microstructural analyses with optical  
109 microscope and cathodoluminescence to unravel different phases of calcite precipitation; (3) calcite  
110 U-Pb LA-ICP-MS dating on veins and slickensides to date fault activity. In most cases, the U-Pb  
111 analyses were performed on calcite crystals showing a homogenous color or undisturbed growth-

112 zoning under cathodoluminescence light, indicating no open-system alteration after calcite  
113 precipitation by late fluid infiltration and/or recrystallization (Figs. S1-S3). Analytical details are  
114 described in the Supplementary Material.

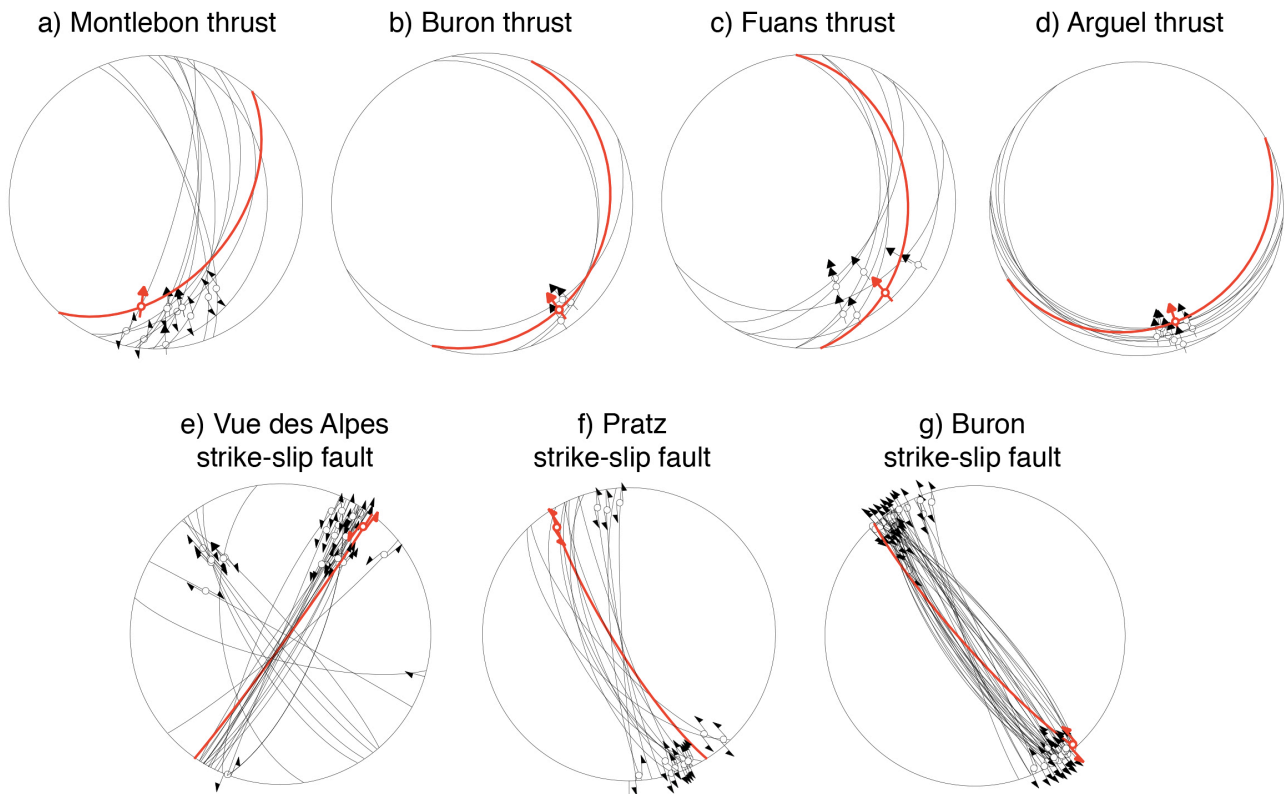
115

## 116 **4. Results**

### 117 *4.1 Structural and microstructural observations*

118 The Montlebon, Buron, Fuans, and Arguel thrusts are NNE-SSW- to SW-NE striking and N-  
119 to NW-verging thrusts (Madritsch et al., 2008; Rime et al., 2019; Smeraglia et al., 2020) (Fig. 2a-d).  
120 More precisely, the Montlebon thrust is characterized by E to ESE-dipping (30-90°) thrust planes  
121 with slickenfibers showing left-lateral transpressional movements with N to NNW tectonic transport  
122 directions (Fig. 2a). The Buron thrust is characterized by E to SE-dipping (20°-30°) thrust planes with  
123 slickenfibers showing left-lateral transpressional movements with NW tectonic transport directions  
124 (Fig. 2b). The Fuans thrust is characterized by E to SE-dipping (20°-40°) thrust planes with  
125 slickenfibers showing left-lateral transpressional movements with NNW to NW tectonic transport  
126 directions (Fig. 2c). The Arguel thrust is characterized by S-dipping (10-30°) thrust planes with  
127 slickenfibers showing right-lateral transpressional movements with NNW tectonic transport  
128 directions (Fig. 2d).

129 The subvertical Vue des Alpes, Pratz, and Buron tear faults show sinistral strike-slip  
130 displacements (Sommaruga, 1997) (Fig. 2de-g). More precisely, the Vue des Alpes strike-slip fault is  
131 characterized by NE-SW-striking subvertical fault planes with slickenfibers showing sinistral  
132 movements and associated NW-SE-striking subvertical fault planes with slickenfibers showing  
133 dextral movements (Fig. 2e). Both the Pratz and Buron strike-slip faults are characterized by NE-SW-  
134 striking subvertical fault planes with slickenfibers showing sinistral movements (Fig. 2f-g).



135

136

137

138

139

140

141

142

143

144

145

146

147

148

149

150

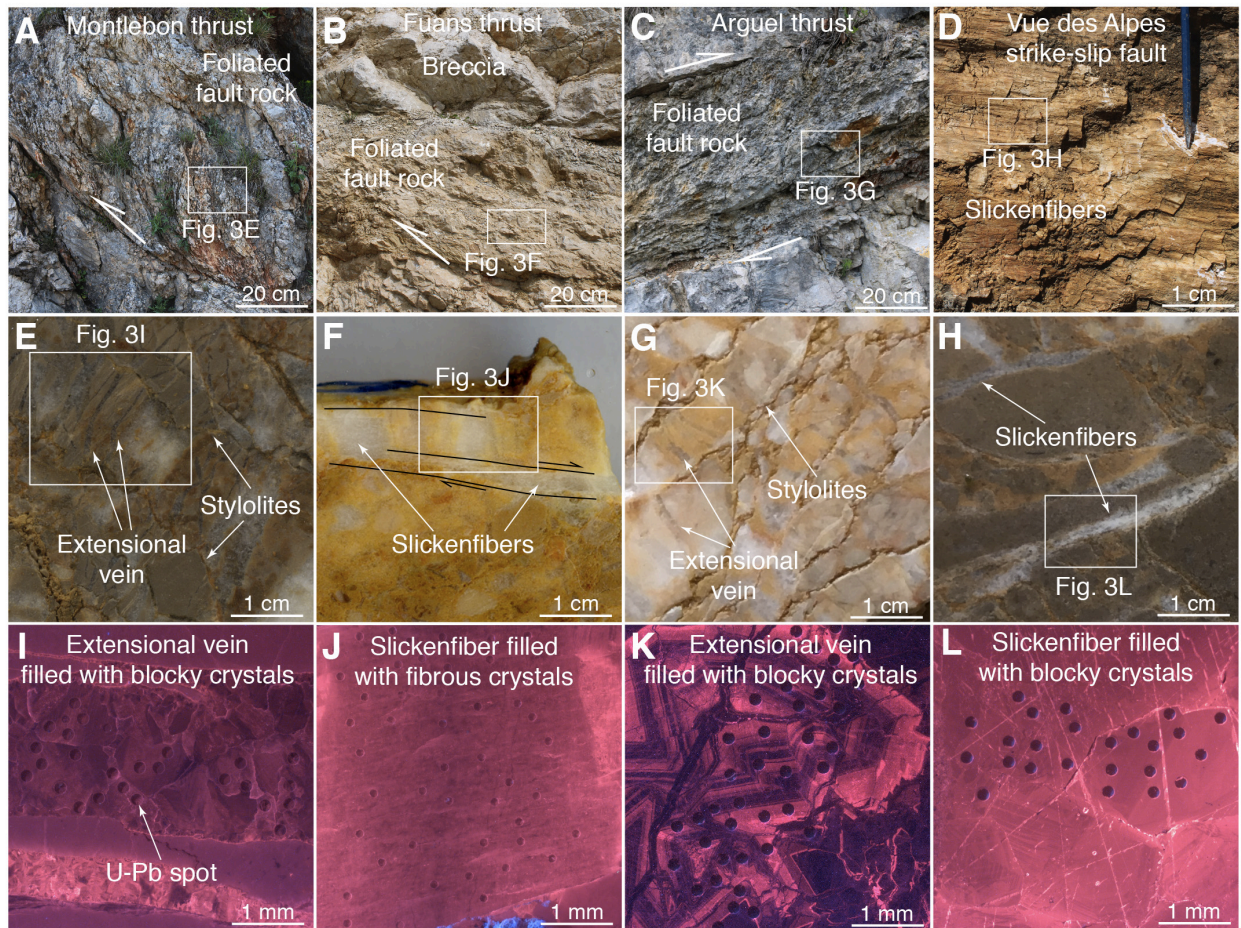
**Figure 2.** Lower Schmidt hemisphere projection of fault-slip data and slip vectors for thrust and strike-slip faults. Dated faults in red. (a) Montlebon thrust. (b) Buron thrust. (c) Fuans thrust. (d) Arguel thrust. (e) Vue des Alpes strike-slip fault. (f) Pratz strike-slip fault. (g) Buron strike-slip fault-

Both thrusts and strike-slip faults cut through Middle-Upper Jurassic and Lower Cretaceous limestones. The fault core zones are characterized by foliated fault rocks cut by sharp fault planes (Fig. 3a-d). Breccia lenses are developed in the Buron thrust core (Fig. 4d). Calcite mineralizations in extensional veins (Buron, Arguel, Montlebon, Vue des Alpes, and Pratz) and in slickenfibers (Fuans, Vue des Alpes, and Pratz) were sampled.

Extensional veins occur in limestone fragments of foliated fault rocks (Fig. 3e,g) and in clasts from breccias (Figs. 3f and 4g). In limestone fragments of foliated fault rocks, extensional veins are oriented perpendicularly to stylolites (Fig. 3e,g), which occur along S- and C-planes. Extensional veins in clasts from breccias show a crackle-like texture and mutually cross-cutting relationships (Fig. 3f). Extensional veins are filled by blocky to elongated-blocky calcite crystals and show syntaxial growth (Figs. 3i-k, 4g, S1a-d, S2a,b,g,h, S3a-h).

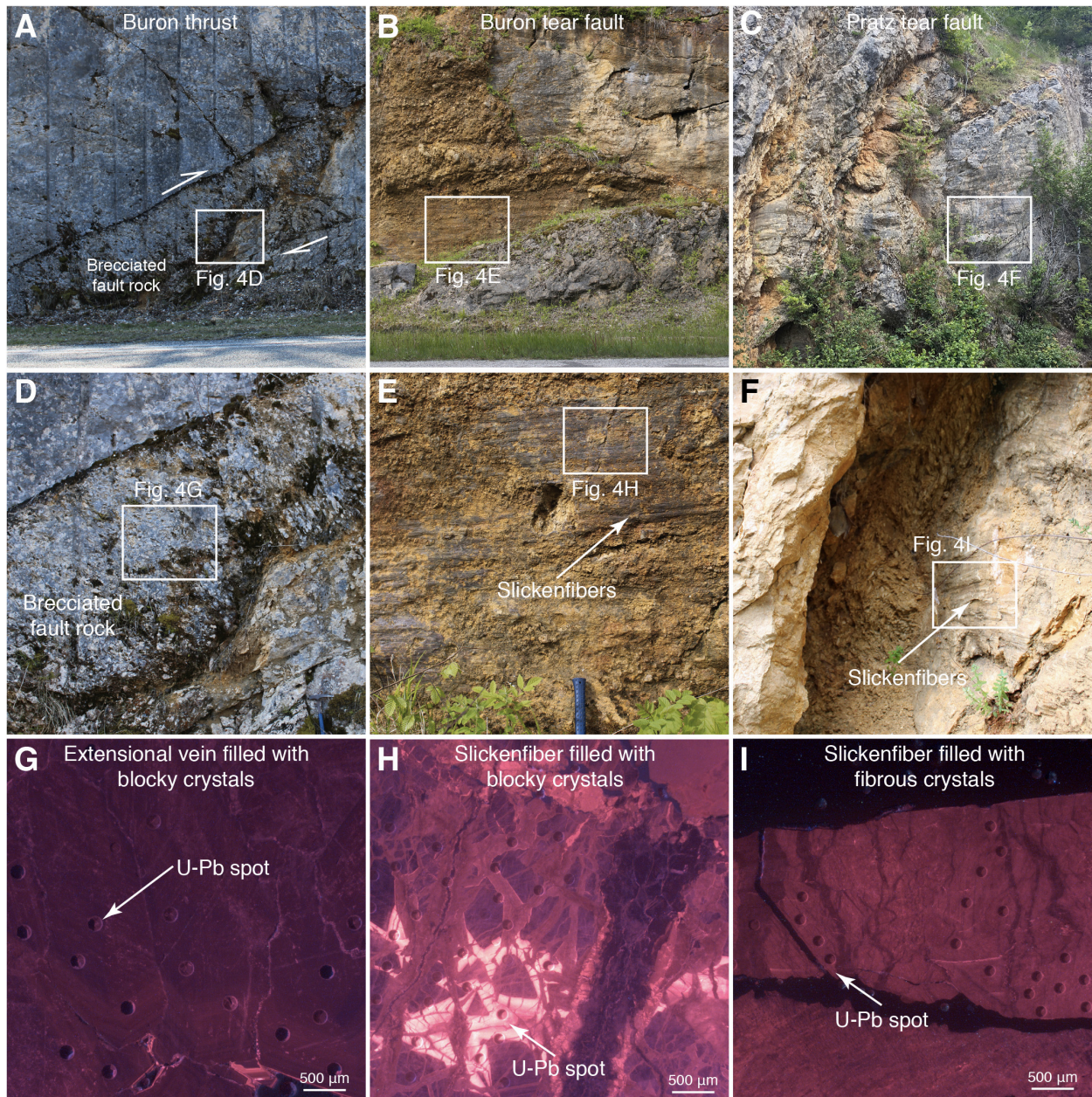
151 The fault planes are coated by slickenfibers (Figs. 3d,h and 4e,f). At the microscale,  
 152 slickenfibers occur in dilational jogs along shear planes (Fig. 3h) and are filled by fibrous calcite  
 153 crystals bounded by sharp shear planes (Figs. 3j, 4i, S1e-h, and S2c-f) and/or by blocky calcite crystals  
 154 (Figs. 3l and 4h). Fibrous crystals are oriented parallel to shear planes.

155 Most of the studied veins and slickenfibers show homogeneous cathodoluminescence colors,  
 156 ranging from bright to dull red, and/or show cathodoluminescence zoning on the same crystal (Figs.  
 157 3i-l, 4g-i, S1a,c,e,g, S2a,c,e,g, and S3a,c,e,g). In places, slickenfibers and extensional veins are cross-  
 158 cut by extensional veins showing black to dull red luminescence colors (Figs. S1e-h, S2c-f, and  
 159 S3a,b,g,h)



160  
 161 **Figure 3.** Foliated fault rocks in the fault core of the Montlebon thrust (a), Arguel thrust (b), and (c) Fuans thrust. (d)  
 162 Detail of minor fault plane along the Vue des Alpes strike-slip fault showing calcite slickenfibers. (e) Hand sample from  
 163 the Montlebon thrust showing host rock sigmoids bounded by stylolites and extensional veins perpendicular to stylolites.  
 164 (f) Hand sample from the Fuans thrust showing host rock sigmoids bounded by stylolites and extensional veins

165 perpendicular to stylolites. **(g)** Hand sample from the Arguel thrust showing extensional veins with crackle-like texture.  
 166 **(h)** Hand sample from a minor fault plane along the Vue des Alpes strike-slip fault showing slickenfibers developed along  
 167 dissolution planes. **(i-l)** Cathodoluminescence microphotographs of thin sections showing extensional veins and  
 168 slickenfibers from the studied faults with ablation craters of the U-Pb analyses.  
 169



170  
 171 **Figure 4.** **(a)** Buron thrust. **(b)** Buron tear fault. **(c)** Pratz tear fault. **(d)** Brecciated fault rocks in the fault core of the  
 172 Buron thrust. **(e)** Brecciated fault rocks cut by sharp fault planes in the fault core of the Buron tear fault. **(f)** Foliated fault  
 173 rock cut by sharp fault planes in the fault core of the Pratz tear fault. **(g-i)** Cathodoluminescence microphotographs of

174 thin sections showing extensional veins and slickenfibers from the studied faults with ablation craters of the U-Pb  
175 analyses.

176

#### 177 4. 2 U-Pb dating

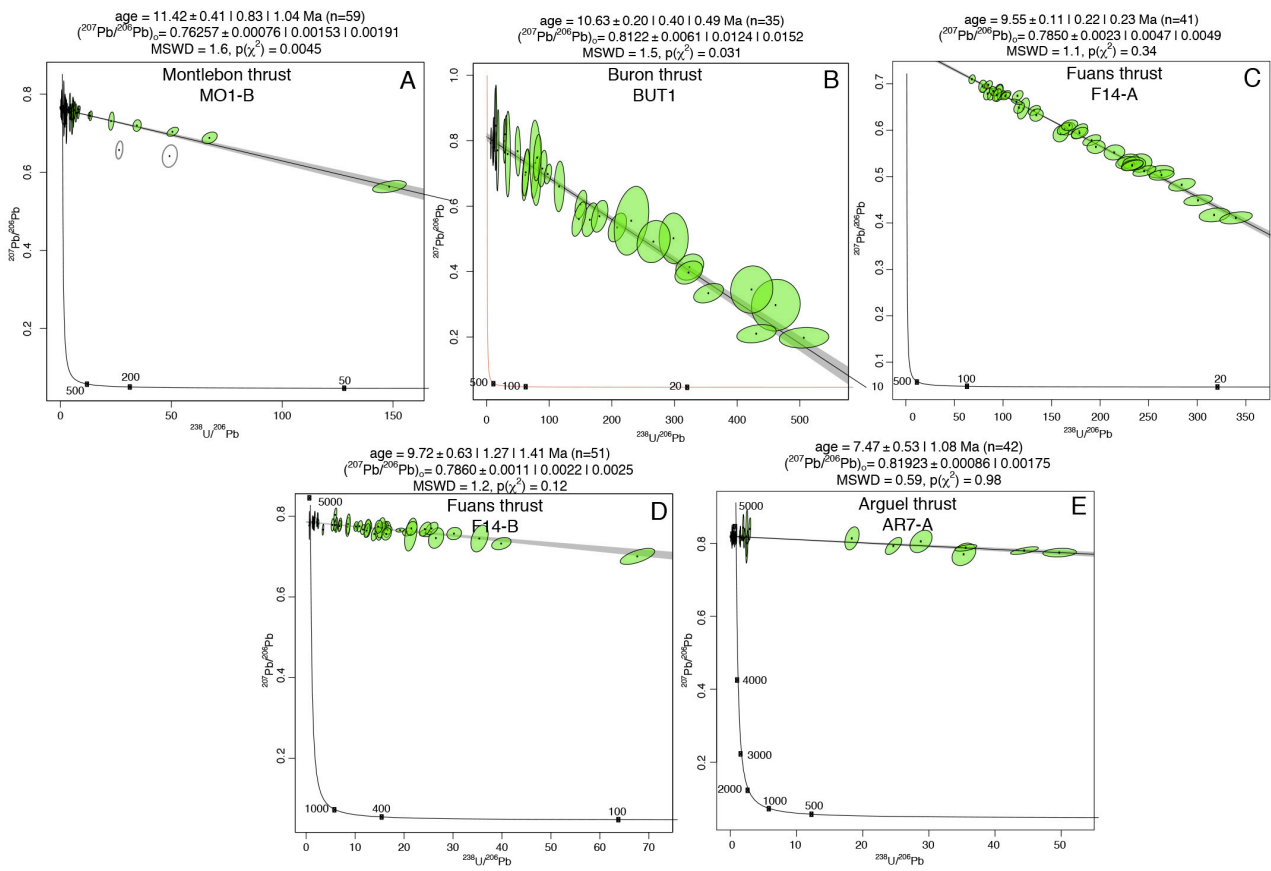
178 A total of 12 reliable lower intercept ages (Figs. 5 and 6) out of 19 analyses (rejected age data  
179 is presented in Fig. S4) are reported with uncertainties at  $2\sigma$  absolute including counting statistics  
180 uncertainties, uncertainty of the primary reference material and inter-session variations (Guillong et  
181 al., 2020). The U-Pb ages indicate different phases of tectonic activity and related calcite precipitation  
182 in the middle Eocene to Pliocene period and also multiple precipitation ages along the same fault  
183 (Supplementary Information Table 1).

184 An extensional vein from the Montlebon thrust shows a Serravallian age of  $11.4 \pm 1.1$  Ma (Fig.  
185 5a). An extensional vein from the Buron thrust shows a Tortonian age of  $10.6 \pm 0.5$  Ma (Fig. 5b).  
186 Two slickenfibers from the Fuans thrust yield Tortonian ages indistinguishable from each other of  
187  $9.7 \pm 1.4$  Ma and  $9.6 \pm 0.3$ , respectively (Fig. 5c,d). An extensional vein from the Arguel thrust shows  
188 a Tortonian-Messinian age of  $7.5 \pm 1.1$  Ma (Fig. 5e). Along the Vue des Alpes strike-slip fault, two  
189 slickenfibers yield Ypresian-Lutetian ages of  $44.7 \pm 2.6$  and  $48.4 \pm 1.5$  Ma (Fig. 6a,b), while an  
190 extensional vein shows a Pliocene age of  $3.9 \pm 2.9$  Ma (Fig. 6c). An extensional vein from the Buron  
191 strike-slip fault shows a Messinian age of  $5.7 \pm 4.7$  Ma (Fig. 6d). One slickenfiber and one extensional  
192 vein from the Pratz strike-slip fault show Tortonian-Messinian ages of  $10.5 \pm 0.4$  and  $9.1 \pm 6.5$  Ma  
193 (Fig. 6f-g), while one slickenfiber shows a younger age of  $4.8 \pm 1.7$  Ma (Fig. 6e). Because of the  
194 common-lead rich  $^{207}\text{Pb}/^{206}\text{Pb}$  compositions, the U-Pb ages of the samples DA2, BUS1, PR1-A, PR2-  
195 2 of the strike-slip faults have larger uncertainties than those of the thrusts.

196

197

## U-Pb ages from thrusts

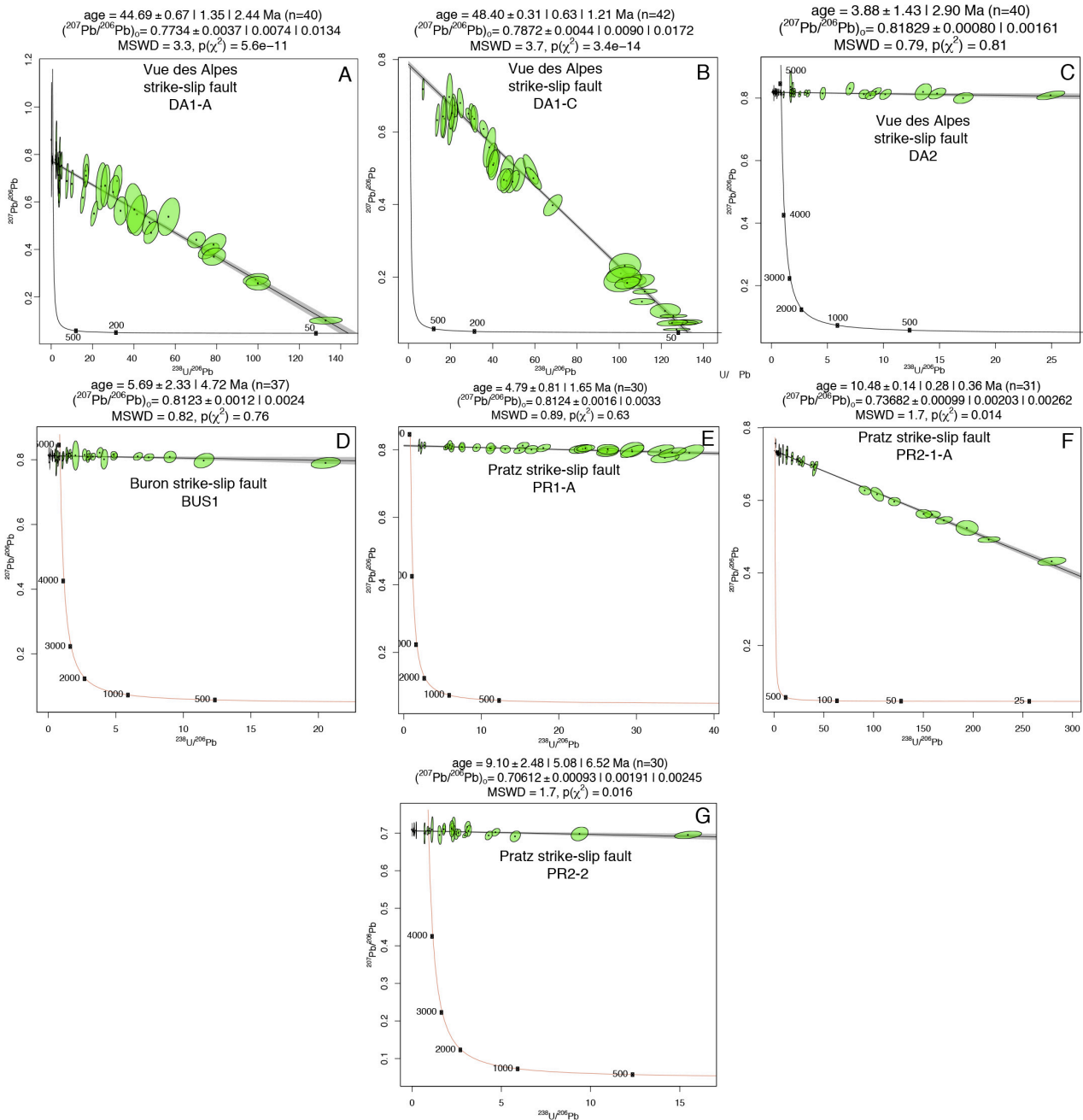


198

199 **Figure 5.** Tera-Wasserburg concordia diagrams of thrust faults. **(a)** Montlebon thrust. **(a)** Buron thrust. **(c,d)** Fuans thrust.

200 **(e)** Arguel thrust.

## U-Pb ages from strike-slip faults



201

202 **Figure 6.** Tera-Wasserburg concordia diagrams of strike-slip faults. (a-c) Vue des Alpes strike-slip fault. (d) Buron strike-  
 203 slip fault. (e-g) Pratz strike-slip fault.

204

## 205 5. Discussion and conclusions

206 Slickenfibers on sharp fault planes are clear evidence of tectonic slip along faults (Figs. 3j-1, 4i,

207 S1e-h, and S2c,f). In particular, blocky and fibrous crystals indicate respectively fast and slow vein

208 opening rates associated with fault slip. Within slickenfibers, calcite crystal precipitated during syn-  
209 to early post-slip fluid influx in newly formed dilational sites formed along undulated and sharp slip  
210 planes ([Gratier and Gamond, 1990](#); [Urai et al., 1991](#); [Holland and Urai, 2010](#); [Fagereng et al., 2010](#);  
211 [Bons et al., 2012](#); [Woodcock et al., 2014](#)). Extensional veins oriented perpendicular to stylolites ([Fig.](#)  
212 [3e,g](#)) are linked to syn-thrusting shortening ([Gratier et al., 2013](#)). The studied veins are therefore  
213 interpreted as the product of tectonic fault slip and their U-Pb ages are considered as representative  
214 of faulting activity.

215 We recognize three regional tectonic phases between the middle Eocene and the Pliocene ([Figs.](#)  
216 [7 and 8](#)), which are linked to the long-lived tectonic activity of the Alpine foreland evolution. The  
217 presented ages should be regarded as minimum ages for the onset of deformation at the studied faults  
218 or as maximum ages for its termination as potentially older or younger deformation phases recorded  
219 by other veins and slickenfibers not sampled and analyzed here may have been missed. As commonly  
220 done in carbonate LA-ICP-MS U-Pb dating, no disequilibrium correction for initial  $^{234}\text{U}/^{238}\text{U}$  and  
221  $^{230}\text{Th}$  was applied. This may cause underestimation of young (<10 Ma) samples ([Roberts et al. 2020](#))  
222 and accordingly, they should be regarded to reflect maximal ages.

223 The U-Pb ages are regionally consistent in terms of the tectonic evolution of the Jura FTB, and  
224 the microstructures of the analyzed veins and slickenfibers indicate precipitation during syn- to early  
225 post-slip fluid influx. However, although U-Pb dating was performed on crystals with no indication  
226 of later open-system alteration based on CL-microscopy, possible late fluid infiltration and calcite  
227 recrystallization cannot be excluded as previously suggested by other studies ([Beaudoin et al., 2018](#);  
228 [Hoareau et al., 2021](#); [Roberts et al., 2020, 2021](#)).

229 Sample BUS1 clearly shows multiple calcite phases indicating vein re-opening and potentially  
230 different ages ([Fig. 4h](#)). However, the Tera-Wasserburg diagram of BUS1 shows a single age trend  
231 with a low MSWD of 0.82 ([Fig. 6d](#)). This would not be observed in a sample that experienced  
232 crystallization at significantly different times. Therefore, sample BUS1 reflects calcite precipitation  
233 within a time interval smaller than what would result in multiple age trends.

234 The oldest tectonic phase is recorded by two horizontal slickenfibers dated at  $44.7 \pm 2.6$  and  
235  $48.4 \pm 1.5$  Ma in Ypresian-Lutetian times (middle Eocene) along the Vue des Alpes strike-slip fault  
236 (Fig. 7). These ages are  $\sim 10$  Ma older than the onset of the extensional tectonic activity in Priabonian  
237 (late Eocene) related to Rhine Graben opening (Sissingh, 1998; Mazurek et al. 2018). The strike-slip  
238 faulting in Eocene times is consistent with fault-slip data of Homberg et al. (1997). We propose that  
239 the Ypresian-Lutetian tectonic activity can be related to the late Mesozoic-Eocene far field tectonic  
240 shortening in the European plate foreland due to the advancing Alpine orogen (Mazurek et al., 2006;  
241 Timar-Geng et al., 2006) (Fig. 8a). However, previous studies suggested that middle Eocene strike-  
242 slip faulting in the Jura area can be also related to the far-field effect of the Pyrenean compression  
243 (Bergerat, 1987; Homberg et al., 2002). The Pyrenean far field effect is also recognized in the Paris  
244 Basin (e.g., Lacombe et al., 1990; Lacombe and Mouthereau, 1999; Lacombe and Obert, 2000), in  
245 eastern France (Lacombe et al., 1993), and even in the United Kingdom (Hibsch et al., 1995) where  
246 Pyrenean-related calcite veins were dated by U-Pb (ages between 55 and 25 Ma; Parrish et al., 2018).  
247 Therefore, we cannot fully distinguish if the strike-slip fault activity during Ypresian-Lutetian times  
248 is related to the Pyrenean or to the Alpine shortening. Further studies are necessary to better constrain  
249 the origin of pre-Miocene fault activity in the European foreland.

250 Structural analyses of the studied thrusts highlight N to NW oriented tectonic transport  
251 directions (Fig. 4a-d) consistent with the regional NW-SE to N-S compressional phase that has  
252 affected the Jura fold and thrust belt since the Miocene (Philippe et al, 1996; Becker, 2000; Homberg  
253 et al., 2002; Ustaszewski and Schmid, 2006; Madritsch et al., 2008; Looser et al., 2021). Although  
254 age uncertainties do not allow a distinction beyond doubt and the limited numbers of U-Pb ages and  
255 studied thrusts provide a limited picture, the Jura imbrication seems to have occurred by in-sequence  
256 thrusting. The oldest observed thrusts ages are Serravallian-Messinian and become progressively  
257 younger moving from the inner (SE) toward the external (NW) part, from  $11.4 \pm 1.1$ ,  $10.6 \pm 0.5$ ,  $9.7$   
258  $\pm 1.4$  and  $9.6 \pm 0.3$  on the same thrust, and  $7.5 \pm 1.1$  Ma, respectively, in the Montlebon, Buron,  
259 Fuans, and Arguel thrusts (Figs. 7 and 8b). These ages are consistent with the time interval of  $\sim 14.5$ -

260 3.3 Ma suggested for thrusting activity from biostratigraphic dating of syn- to post-tectonic sediments  
261 ([Becker, 2000 and references therein](#)) and from calcite U-Pb ages of thrust activity in the eastern Jura  
262 FTB ([Looser et al., 2021](#)) ([Fig. 7](#)).

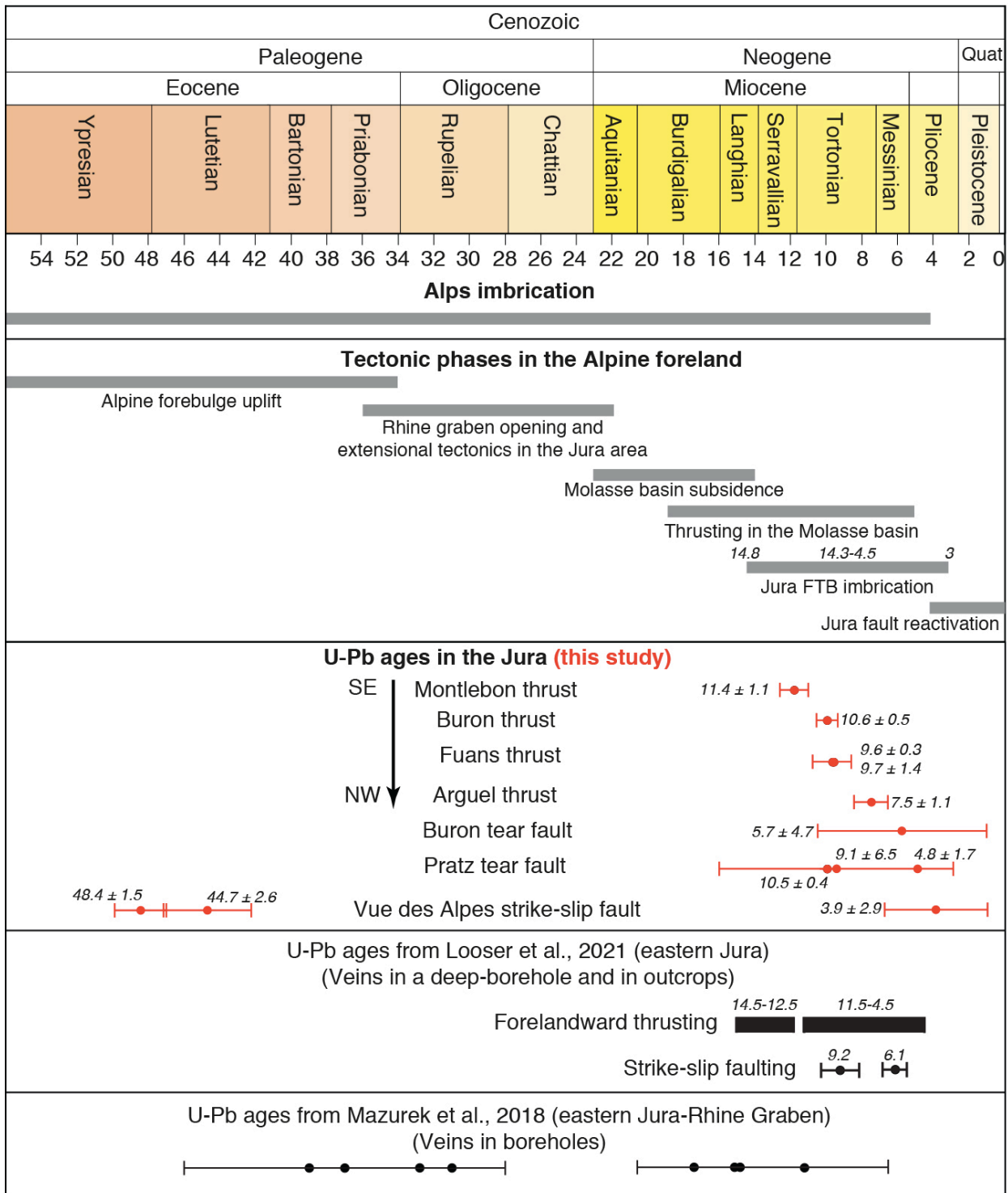
263 Previous studies interpreted the subvertical strike-slip faults in the Jura FTB as tear faults, with  
264 activity during thrusting and folding ([Sommaruga, 1997; Looser et al., 2021](#)). Our structural analyses  
265 and U-Pb ages from the studied strike-slip faults support this interpretation. In particular, strike-slip  
266 faults are subvertical and are roughly parallel or oblique to the regional transport directions inferred  
267 from thrust kinematics (compare tectonic transport directions of [Fig. 4a-d](#) with those of [Fig. 4f,g](#)), a  
268 common feature of tear faults ([Twiss and Moores, 1992](#)).

269 The Buron thrust, active at  $10.6 \pm 0.5$  Ma, was cross-cut by the Buron tear fault  $\sim 5$  Ma later, at  
270  $5.7 \pm 4.7$  Ma ([Figs. 7 and 8c](#)). The Pratz tear fault was active at  $10.5 \pm 0.4$  and  $9.1 \pm 6.5$  Ma, indicating  
271 tear faulting generation during coeval thrust propagation, and further late-orogenic re-activation at  
272  $4.8 \pm 1.7$  Ma ([Figs. 7 and 8b](#)). These data indicate that tear faulting occurred during syn- to late-  
273 orogenic times ([Fig. 8b,c](#)). In addition, a late-orogenic phase is recorded by an extensional vein from  
274 the Vue des Alpes strike-slip fault showing a Pliocene age of  $3.9 \pm 2.9$  Ma ([Fig. 7](#)). This age has been  
275 measured on an extensional vein that cannot be directly related to fault slip. Therefore, we cannot  
276 completely exclude that this age represents a late alteration event not directly linked to fault slip  
277 during the Pliocene. However, the  $3.9 \pm 2.9$  Ma age is consistent with late orogenic deformation  
278 between 4.2 and 2.9 Ma documented in the frontal part of the Jura FTB ([Madritsch et al., 2008 and](#)  
279 [references therein](#)). The  $3.9 \pm 2.9$  Ma age from the Vue des Alpes strike-slip fault is  $\sim 40$  Ma younger  
280 than the middle Eocene ages ( $44.7 \pm 2.6$  and  $48.4 \pm 1.5$  Ma) measured on the same fault, suggesting  
281 the reactivation of the Vue des Alpes strike-slip fault during late Jura shortening. This inference is  
282 also consistent with field cross-cutting relationships indicating re-activation of pre-existing strike-  
283 slip faults as tear faults ([Homberg et al., 1997](#)).

284 We consider the retrieved age as fault re-activation of the Vue des Alpes strike-slip fault and  
285 relate it to a stress change from pure compression to strike-slip state of stress coupled with the

286 occurrence of an inherited strike-slip fault favorably oriented with respect to the regional stress field.  
287 This stress change associated with tear fault development can be related to progressive fold-and-thrust  
288 belt thickening initiating only after ~4.5 Ma (Looser et al., 2021 and references therein), which led to  
289 an increase in the principal vertical stress ( $\sigma_3$ ) and a switch between  $\sigma_3$  and  $\sigma_2$  (Ferril  
290 et al., 2021). Shortening is still active in the Jura FTB and tear faults (also re-activated tear faults) are  
291 seismogenic (Thouvenot et al., 1998).

292 The presented tectonic reconstruction depicts a stable evolution of the Jura FTB wedge by  
293 possible in-sequence thrusting consistent with thrust imbrication above the low-friction décollement  
294 consisting of evaporites (Fig. 8a-c). Contrarily, out-of-sequence thrusting occurred as late as in  
295 Messinian-early Pliocene times in the proximal Molasse Basin (Von Hagke et al., 2012, 2014) and in  
296 the Alps (Bellahsen et al., 2014). This tectonic framework suggests a stable topographic evolution of  
297 the critical taper and topographic profile of the Jura fold-and-thrust belt. Finally, this study constrains  
298 a long-lived polyphase tectonic history of the northwestern Alpine foreland system along the  
299 convergent boundary between European and African plates from the middle Eocene to the Pliocene.



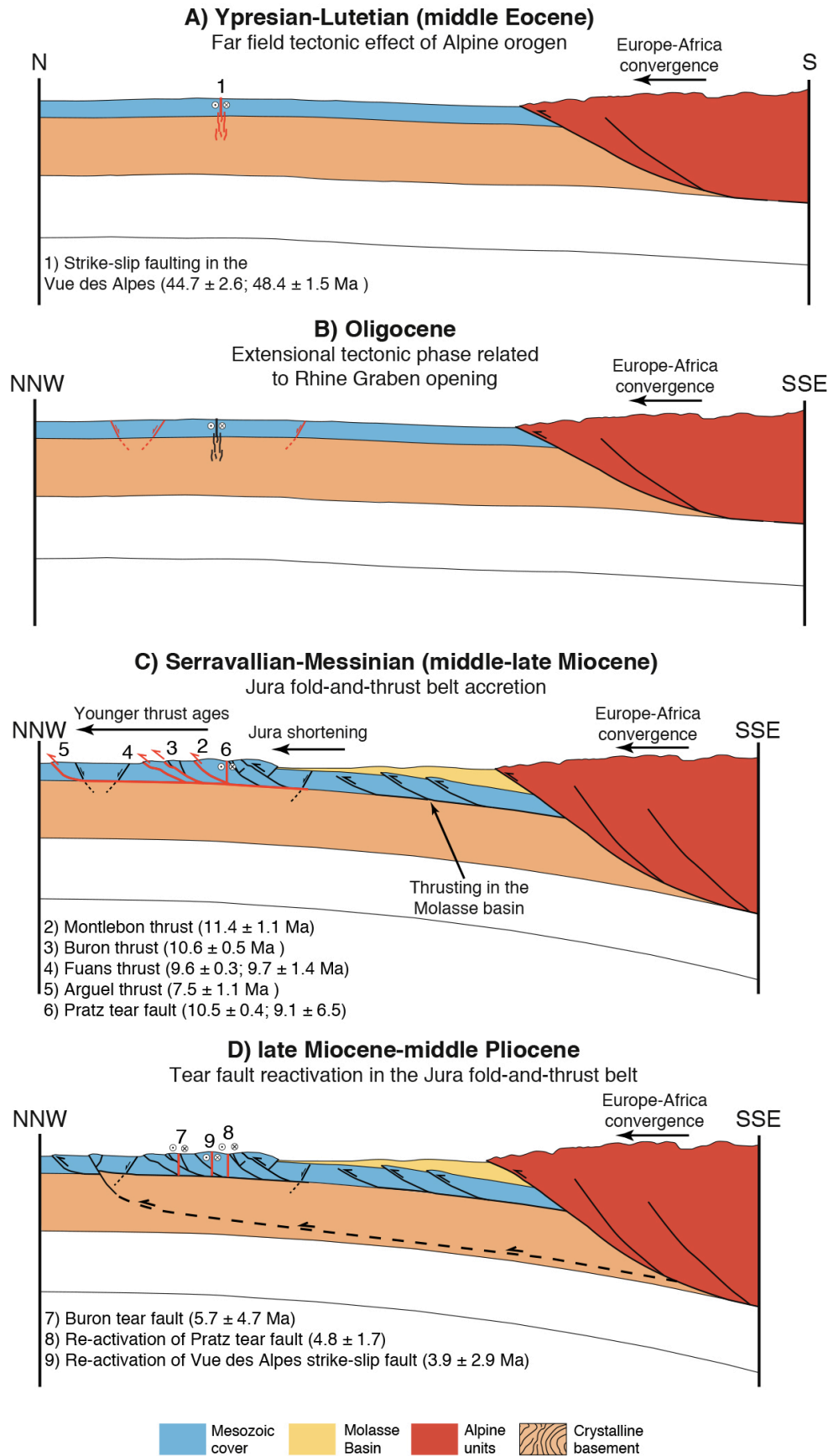
300

301

302

303

**Figure 7.** Main tectonic phases in the Alps and in the Alpine foreland. Age constraints shown as grey bars are from Burkhard and Sommaruga (1998), Ustaszewski et al. (2006), Madritsch et al. (2008), Bellahsen et al. (2014), and Von Hagke et al. (2014). For calcite U-Pb data, all uncertainties are represented as  $2\sigma$ .



304

305 **Figure 8. (a-d)** Schematic reconstruction of the main tectonic phases dated in the Jura area in the regional context of the  
306 Alpine foreland system evolution.

307 **ACKNOWLEDGEMENT**

308 We thank CASP (<https://www.casp.org.uk/>) for financial support during fieldwork activity by  
309 the Andy Whitham Fieldwork Award 2019 to L. Smeraglia. Financial support by Borsa di  
310 Perfezionamento Estero 2017 (Sapienza) to L. Smeraglia, UMR 6249 and OSU Theta projects to O.  
311 Fabbri and F. Choulet are acknowledged. U-Pb analyses were funded by the Swiss National Science  
312 Foundation project number 200021\_169849 to S. M. Bernasconi. We thank J. Mosar, M. Schori, A.  
313 Sommaruga, C. Mottran, L. Weiss, and C. Von Hagke for constructive discussions and suggestions,  
314 also during fieldwork. We thank the Editor Susanne Buiter and two reviewers Olivier Lacombe and  
315 Nick Roberts for their constructive comments that helped to improve the manuscript.

316

317 **REFERENCES**

- 318 Affolter, T., and Gratier, J. P.: Map view retrodeformation of an arcuate fold-and-thrust belt: The Jura  
319 case. *Journal of Geophysical Research: Solid Earth*, 109(B3), 2004.
- 320 Beaudoin, N., and Lacombe, O.: Recent and future trends in paleopiezometry in the diagenetic  
321 domain: Insights into the tectonic paleostress and burial depth history of fold-and-thrust belts  
322 and sedimentary basins. *Journal of Structural Geology*, 114, 357-365, 2018.
- 323 Beaudoin, N., Leprêtre, R., Bellahsen, N., Lacombe, O., Amrouch, K., et al.: Structural and  
324 microstructural evolution of the Rattlesnake Mountain Anticline (Wyoming, USA): new  
325 insights into the Sevier and Laramide orogenic stress build-up in the Bighorn Basin.  
326 *Tectonophysics*, 576, 20-45, 2012.
- 327 Beaudoin, N., Lacombe, O., Roberts, N. M., and Koehn, D.: U-Pb dating of calcite veins reveals  
328 complex stress evolution and thrust sequence in the Bighorn Basin, Wyoming, USA. *Geology*,  
329 46(11), 1015-1018, 2018.
- 330 Becker, A.: The Jura Mountains - an active foreland fold-and-thrust belt?. *Tectonophysics*, 321(4),  
331 381-406, 2000.

332 Bellahsen, N., Mouthereau, F., Boutoux, A., Bellanger, M., Lacombe, O., Jolivet, L., and Rolland,  
333 Y. : Collision kinematics in the western external Alps. *Tectonics*, 33(6), 1055-1088, 2014.

334 Bergerat, F.: Stress fields in the European platform at the time of Africa-Eurasia collision. *Tectonics*  
335 6, 99-132, 1987.

336 Bons, P. D., Elburg, M. A., and Gomez-Rivas, E.: A review of the formation of tectonic veins and  
337 their microstructures. *Journal of Structural Geology*, 43, 33-62, 2012.

338 Carminati E., Aldega L., Smeraglia L., Scharf A., Mattern F., Albert R., and Gerdes A.: Tectonic  
339 evolution of the Northern Oman Mountains, part of the Strait of Hormuz Syntaxis: new  
340 structural and paleothermal analyses and U-Pb dating of synkinematic calcite. *Tectonics* 39,  
341 e2019TC005936, 2020.

342 Craig, M. S., and Warvakai, K.: Structure of an active foreland fold and thrust belt, Papua New  
343 Guinea. *Australian Journal of Earth Sciences*, 56(5), 719-738, 2009.

344 Craddock, J. P., Jackson, M., van der Pluijm, B. A., & Versical, R. T.: Regional shortening fabrics in  
345 eastern North America: Far-field stress transmission from the Appalachian-Ouachita Orogenic  
346 Belt. *Tectonics*, 12(1), 257-264, 1993.

347 Fagereng, Å., Remitti, F., and Sibson, R. H.: Shear veins observed within anisotropic fabric at high  
348 angles to the maximum compressive stress. *Nature Geoscience*, 3(7), 482, 2010.

349 Ferril, D.A., Smart, K.J., Cawood, A.J., Morris, A.P.: The fold-thrust belt stress cycle: Superposition  
350 of normal, strike-slip, and thrust faulting deformation regimes. *Journal of Structural Geology*  
351 148, 104362, 2021.

352 Goodfellow, B. W., Viola, G., Bingen, B., Nuriel, P., and Kylander-Clark, A. R.: Paleocene faulting  
353 in SE Sweden from U–Pb dating of slickenfiber calcite. *Terra Nova*, 29(5), 321-328, 2017.

354 Gratier, J. P., and Gamond, J. F.: Transition between seismic and aseismic deformation in the upper  
355 crust. *Geological Society, London, Special Publications*, 54(1), 461-473, 1990.

356 Gratier, J.P., Thouvenot, F., Jenatton, L., Tourette, A., Doan, M.L., Renard, F.: Geological control of  
357 the partitioning between seismic and aseismic sliding behaviours in active faults: evidence from  
358 the Western Alps, France. *Tectonophysics* 600, 226-242, 2013.

359 Gruber, M.: Structural Investigations of the Western Swiss Molasse Basin - From 2D Seismic  
360 Interpretation to a 3D Geological Model. *GeoFocus*, 41, 190 pp, 2017.

361 Guillong, M., Wotzlaw, J., Looser, N., & Laurent, O. (2020). Evaluating the reliability of U–Pb laser  
362 ablation inductively coupled plasma mass spectrometry (LA-ICP-MS) carbonate  
363 geochronology: Matrix issues and a potential calcite validation reference material.  
364 *Geochronology*, 2, 155–167. <https://doi.org/10.5194/gchron-2-155-2020>.

365 Hansman, R. J., Albert, R., Gerdes, A., and Ring, U.: Absolute ages of multiple generations of brittle  
366 structures by U-Pb dating of calcite. *Geology*, 46(3), 207-210, 2018.

367 Hibschi, C., Jarrige, J. J., Cushing, E. M., and Mercier, J.: Palaeostress analysis, a contribution to the  
368 understanding of basin tectonics and geodynamic evolution. Example of the Permian/Cenozoic  
369 tectonics of Great Britain and geodynamic implications in western Europe. *Tectonophysics*,  
370 252(1-4), 103-136, 1995.

371 Hoareau, G., Crognier, N., Lacroix, B., Aubourg, C., Roberts, N. M., et al.: Combination of  $\Delta 47$  and  
372 U-Pb dating in tectonic calcite veins unravel the last pulses related to the Pyrenean Shortening  
373 (Spain). *Earth and Planetary Science Letters*, 553, 116636, 2021.

374 Holland, M., and Urai, J. L.: Evolution of anastomosing crack–seal vein networks in limestones:  
375 Insight from an exhumed high-pressure cell, Jabal Shams, Oman Mountains. *Journal of*  
376 *Structural Geology*, 32(9), 1279-1290, 2010.

377 Homberg, C., Hu, J. C., Angelier, J., Bergerat, F., and Lacombe, O.: Characterization of stress  
378 perturbations near major fault zones: insights from 2-D distinct-element numerical modelling  
379 and field studies (Jura mountains). *Journal of Structural Geology*, 19(5), 703-718, 1997.

380 Homberg, C., Bergerat, F., Philippe, Y., Lacombe, O., and Angelier, J.: Structural inheritance and  
381 Cenozoic stress fields in the Jura fold-and-thrust belt (France). *Tectonophysics*, 357(1-4), 137-  
382 158, 2002.

383 Jordan, P.: Evidence for large-scale decoupling in the Triassic evaporites of Northern Switzerland:  
384 an overview. *Eclogae Geologicae Helvetiae*, 85, 677–693, 1992.

385 Lacombe, O., Angelier, J., Laurent, P., Bergerat, F., and Tournier, C.: Joint analyses of calcite twins  
386 and fault slips as a key for deciphering polyphase tectonics: Burgundy as a case study.  
387 *Tectonophysics*, 182(3-4), 279-300, 1990.

388 Lacombe, O., Angelier, J., Byrne, D., and Dupin, J. M.: Eocene-Oligocene tectonics and kinematics  
389 of the Rhine-Saone continental transform zone (eastern France). *Tectonics*, 12(4), 874-888,  
390 1993.

391 Lacombe, O., and Mouthereau, F.: What is the real front of orogens? The Pyrenean orogen as a case  
392 study. *Comptes Rendus de l'Academie des Sciences Series IIA Earth and Planetary Science*,  
393 329(12), 889-896, 1999.

394 Lacombe, O., & Mouthereau, F. (2002). Basement-involved shortening and deep detachment  
395 tectonics in forelands of orogens: Insights from recent collision belts (Taiwan, Western Alps,  
396 Pyrenees). *Tectonics*, 21(4), 12-1.

397 Lacombe, O., and Obert, D.: Structural inheritance and cover deformation: Tertiary folding and  
398 faulting in, the western Paris Basin. *Comptes rendus de l'academie des sciences serie ii*  
399 *fascicule a-sciences de la terre et des planetes*, 330(11), 793-798, 2000.

400 Lacombe, O., Lavé, J., Roure, F. M., and Vergés, J. (Eds.): Thrust belts and foreland basins: From  
401 fold kinematics to hydrocarbon systems. Springer Science & Business Media, 2007.

402 Lacombe, O., and Bellahsen, N.: Thick-skinned tectonics and basement-involved fold–thrust belts:  
403 insights from selected Cenozoic orogens. *Geological Magazine*, 153, 763-810, 2016.

404 Looser, N., Madritsch, H., Guillong, M., Laurent, O., Wohlwend, S., & Bernasconi, S. M. (2021).  
405 Absolute age and temperature constraints on deformation along the basal décollement of the

406 Jura fold-and- thrust belt from carbonate U-Pb dating and clumped isotopes. *Tectonics*, 40,  
407 e2020TC006439. <https://doi.org/10.1029/2020TC006439>

408 Madritsch, H., Schmid, S. M., and Fabbri, O.: Interactions between thin- and thick-skinned tectonics  
409 at the northwestern front of the Jura fold-and-thrust belt (eastern France). *Tectonics*, 27, 1-31,  
410 2008.

411 Mazurek, M., Davis, D. W., Madritsch, H., Rufner, D., Villa, I. et al. (2018). Veins in clay-rich  
412 aquitards as records of deformation and fluid-flow events in northern Switzerland. *Applied*  
413 *Geochemistry*, 95, 57-70, 2008.

414 Mazurek, M., Hurford, A. J., and Leu, W.: Unravelling the multi-stage burial history of the Swiss  
415 Molasse Basin: integration of apatite fission track, vitrinite reflectance and biomarker  
416 isomerisation analysis. *Basin Research*, 18, 27–50, 2006.

417 [Merle, O., & Michon, L. \(2001\). The formation of the West European Rift; a new model as](#)  
418 [exemplified by the Massif Central area. \*Bulletin de la Société géologique de France\*, 172\(2\),](#)  
419 [213-221.](#)

420 Mosar, J.: Present-day and future tectonic underplating in the western Swiss Alps: reconciliation of  
421 basement/wrench-faulting and décollement folding of the Jura and Molasse basin in the Alpine  
422 foreland. *Earth and Planetary Science Letters*, 173, 143-155, 1999.

423 Nuriel, P., Weinberger, R., Kylander-Clark, A. R. C., Hacker, B. R., and Craddock, J. P.: The onset  
424 of the Dead Sea transform based on calcite age-strain analyses. *Geology*, 45(7), 587-590, 2017.

425 Parrish, R. R., Parrish, C. M., and Lasalle, S.: Vein calcite dating reveals Pyrenean orogen as cause  
426 of Paleogene deformation in southern England. *Journal of the Geological Society*, 175(3), 425-  
427 442, 2018.

428 Philippe, Y., Colletta, B., Deville, E., and Mascle, A.: The Jura fold-and-thrust belt: a kinematic  
429 model based on map-balancing. *Mémoires du Muséum national d'histoire naturelle*, 170, 235-  
430 261, 1996.

431 Pfiffner, O. A.: *Geology of the Alps*. Chichester: John Wiley & Son, 2014.

- 432 Rime, V., Sommaruga, A., Schori, M., and Mosar, J. : Tectonics of the Neuchâtel Jura Mountains:  
433 insights from mapping and forward modelling. *Swiss Journal of Geosciences*, 112, 563-578,  
434 2019.
- 435 Roberts, N. M., Drost, K., Horstwood, M. S., Condon, D. J., Chew, D., Drake, H., and Haslam, R.:  
436 Laser ablation inductively coupled plasma mass spectrometry (LA-ICP-MS) U-Pb carbonate  
437 geochronology: strategies, progress, and limitations. *Geochronology*, 2(1), 33-61, 2020.
- 438 Roberts, N. M., Žák, J., Vacek, F., and Sláma, J.: No more blind dates with calcite: Fluid-flow vs.  
439 fault-slip along the Očkov thrust, Prague Basin. *Geoscience Frontiers*, 12(4), 101143, 2021.
- 440 Sissingh, W.: Comparative Tertiary stratigraphy of the Rhine Graben, Bresse Graben and Molasse  
441 Basin: correlation of Alpine foreland events. *Tectonophysics*, 300, 249–28, 1998.
- 442 Smeraglia, L., Aldega, L., Billi, A., Carminati, E., Di Fiore, F., Gerdes, A., and Vignaroli, G.:  
443 Development of an Intrawedge Tectonic Mélange by Out-of-Sequence Thrusting, Buttressing,  
444 and Intraformational Rheological Contrast, Mt. Massico Ridge, Apennines, Italy. *Tectonics*,  
445 38(4), 1223-1249, 2019.
- 446 Smeraglia, L., Fabbri, O., Choulet, F., Buatier, M., Boulvais, P., Bernasconi, S.M., and Castorina, F.:  
447 Syntectonic fluid flow and deformation mechanisms within the frontal thrust of foreland fold-  
448 and-thrust belt: Example from the Internal Jura, Eastern France. *Tectonophysics*, 778,  
449 <https://doi.org/10.1016/j.tecto.2019.228178>, 2020.
- 450 Sommaruga, A.: Geology of the Central Jura and the Molasse basin: New insight into an evaporite-  
451 based foreland fold and thrust belt. *Mémoires de la Société Neuchâteloise de Sciences*  
452 *Naturelles*, 12, pp. 176, 1997.
- 453 Sommaruga, A., Mosar, J., Schori, M., and Gruber, M.: The role of the Triassic evaporites underneath  
454 the North Alpine foreland. In Soto, J., Flinch, J., and Tari, G., (Ed.), *Permo- Triassic salt*  
455 *provinces of Europe, North Africa and the Atlantic Margins: tectonics and hydrocarbon*  
456 *potential*, chapter 22 (IV). Elsevier, 2017.

- 457 Thouvenot, F., Fréchet, J., Tapponnier, P., Thomas, J. C., Le Brun, B., Ménard, G., and Paul, A.: The  
458 ML 5.3 Epagny (French Alps) earthquake of 1996 July 15: a long-awaited event on the Vuache  
459 Fault. *Geophysical Journal International*, 135(3), 876-892, 1998.
- 460 Timar-Geng, Z., Fu¨genschuh, B., Wetzel, A., and Dresmann, H.: The low temperature thermal  
461 history of northern Switzerland as revealed by fission track analysis and inverse thermal  
462 modelling. *Eclogae Geologicae Helvetiae*, 99, 255–270, 2006.
- 463 Twiss, R. J., and Moores, E. M.: *Structural geology*. Macmillan, 1992.
- 464 Urai, J. L., Williams, P. F., and Van Roermund, H. L. M.: Kinematics of crystal growth in syntectonic  
465 fibrous veins. *Journal of Structural Geology*, 13(7), 823-836, 1991.
- 466 Ustaszewski, K., and Schmid, S. M.: Control of preexisting faults on geometry and kinematics in the  
467 northernmost part of the Jura fold-and-thrust belt. *Tectonics*, 25, 1-26, 2006.
- 468 Van der Pluijm, B. A., Hall, C. M., Vrolijk, P. J., Pevear, D. R., and Covey, M. C.: The dating of  
469 shallow faults in the Earth's crust. *Nature*, 412(6843), 172-175, 2001.
- 470 Vergés, J., Muñoz, J. A., and Martínez, A.: South Pyrenean fold and thrust belt: The role of foreland  
471 evaporitic levels in thrust geometry. In *Thrust tectonics*, 255-264. Springer, Dordrecht, 1992.
- 472 Von Hagke, C., Cederbom, C. E., Oncken, O., Stöckli, D. F., Rahn, M. K., and Schlunegger, F.:  
473 Linking the northern Alps with their foreland: The latest exhumation history resolved by low-  
474 temperature thermochronology. *Tectonics*, 31(5), 2012.
- 475 Von Hagke, C., Oncken, O., Ortner, H., Cederbom, C. E., and Aichholzer, S.: Late Miocene to present  
476 deformation and erosion of the Central Alps—Evidence for steady state mountain building from  
477 thermokinematic data. *Tectonophysics*, 632, 250-260, 2014.
- 478 Vrolijk, P., Pevear, D., Covey, M., and LaRiviere, A.: Fault gouge dating: history and evolution. *Clay*  
479 *Minerals*, 53(3), 305-324, 2018.
- 480 Woodcock, N. H., Miller, A. V. M., & Woodhouse, C. D.: Chaotic breccia zones on the Pembroke  
481 Peninsula, south Wales: Evidence for collapse into voids along dilational faults. *Journal of*  
482 *Structural Geology*, 69, 91-107, 2014.

